A Multi-matrix E-nose with Optimal Multi-ranged AFE Circuit for Human Volatilome Fingerprinting

Antonio Vincenzo Radogna, *Member, IEEE*, Giuseppe Grassi, *Senior Member, IEEE*, Stefano D'Amico, *Senior Member, IEEE*, Pietro Aleardo Siciliano, Angiola Forleo, Simonetta Capone

***Abstract*— Since hundreds of volatile organic compounds (VOCs) produced by cell metabolism and released into the blood are excreted through exhaled breath or body fluids, the volatile composition (volatilome) of human samples reflects a subject's state of health and early signals any abnormal deviation from healthy to disease. The chemical volatilomic profile of biological matrices can be transduced in a digital fingerprint by low cost and easy-to-use electronic nose (e-nose) devices based on gas sensor arrays. The e-noses can be used to aid clinical diagnosis supporting conventional diagnostic methods that sometimes require expensive or invasive medical procedures and delays in diagnoses. In this paper, an e-nose devoted to the human volatilome fingerprinting is presented. The device, code-named SPYROX, adopts an array of 8 metal-oxide (MOX) gas sensors and it is able to analyze response signals from different matrices (multi-matrix samples), dealing with exhaled breath and headspace analysis of human biological samples. While other works in literature neglect the design of the interface circuit, here an optimal multi-ranged analog front-end (AFE) circuit is proposed. It aims to the optimization of the read-out sensitivity which, ultimately, leads to accurate training datasets and, consequently, to high classification scores. Finally, the efficacy of the device is proved by testing both chemical standards and mixtures. As a result, a classification accuracy of 100% is achieved with a linear discriminant model. The experimental results give a proof on the system's efficacy to the fingerprint analysis of complex gas mixtures, which are typical of human volatilome.**

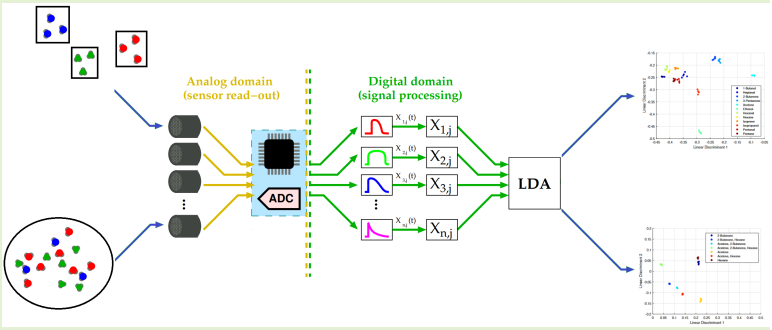

***Index Terms*— electronic nose, sensor systems and applications, chemical sensors, biomedical electronics, analog front-end**

I. Introduction

According to the European Cancer Information System (ECIS), the burden of cancer is increasing in the EU, mainly driven by ageing in the population. New cases reached 2.7 million in 2022, of which the most common were breast cancer for women and prostate cancer for men with incidences of 29% and 22.4%, respectively [1]. Although gold standard methods, such as laboratory tests of biological samples, computed tomography (CT), magnetic resonance imaging (MRI), give the results with the highest possible accuracy in the diagnosis process, in many cases such results are produced too late for an effective cure. Therefore, to significantly improve patients' chances of survival, there is an urgent need for new early-stage cancer detection, screening, and diagnostics tests. The medical and scientific communities are working together to develop fast, low cost, low-power, portable, and non-invasive diagnostic instruments, which can be accepted by the population, easy to access and widespread in health systems, overcoming all the barriers that cause a delay in cancer diagnosis. Electronic noses (e-noses), devices based on gas sensor arrays, constitute a recognized technology that is mature enough to enter clinical practice by satisfying all the above-mentioned requirements [2]–[5]. An e-nose, whose general architecture is depicted in Fig. 1, is an electronic sensing device intended to detect odors or flavors as global fingerprint with no separative mechanism. The expression "electronic sensing" refers to the capability of mimic olfactory sense using sensor arrays, generating signal patterns that are used for characterizing odors and pattern recognition systems. In the figure, the sensor array of the e-nose is exposed to a complex odor j. The electric signals from the sensors are conditioned by the analog front-end (AFE) circuit and then converted from the analog domain to

This work was supported by the *PRO(wellbeing)STATE* Innonetwork project, funded by Apulia region, Italy (code: WF8B9E9).

A.V. Radogna is with Department of Experimental Medicine, University of Salento, Lecce, Italy (e-mail: antonio.radogna@unisalento.it).

G. Grassi and S. D'Amico are with Department of Engineering for Innovation, University of Salento, Lecce, Italy (e-mails: giuseppe.grassi@unisalento.it, stefano.damico@unisalento.it).

P.A. Siciliano, A. Forleo, and S. Capone are with Institute for Microelectronics and Microsystems (IMM), National Research Council (CNR), Lecce, Italy (e-mails: pietroaleardo.siciliano@cnr.it, angiola.forleo@cnr.it, simonetta.capone@cnr.it).

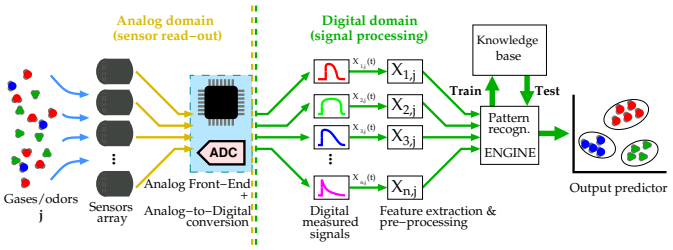

Fig. 1. Architecture of an e-nose.

the digital domain by means of an analog-to-digital converter (ADC). The digitized signals are pre-processed to extract the sensor features, i.e., $x_{n,j}$ in Fig. 1. These are the relevant features from the temporal sensor curves, that will be used as inputs for the pattern recognition analysis. The latter aims to determine the underlying relationships between one set of independent variables, i.e., the outputs from a sensor array, and another set of dependent variables, i.e., odor classes and/or component concentrations by using classifier algorithms and statistical multivariate analysis. The goal is to identify, classify, and quantify, when possible, different odor classes of unknown odors. The rationale behind the use of e-noses in diagnostics is their ability to provide a health-related fingerprint of the volatile organic compounds (VOCs) of exhaled breath and body fluids (blood, urine, saliva, semen, etc.) [6]–[9]. VOCs are metabolites resulting from cellular biochemical activity; they are present in all biological matrices as well as in exhaled alveolar breath where they are excreted at the very onset of any disease. The volatilomes, i.e., the entire VOC profiles of human biosamples, represent valuable volatile signatures of health status that can be used to detect early stages of disease. In addition, the volatilome also contains exogenously derived compounds that do not derive from metabolic processes (e.g., environmental contaminants), but can participate in eliciting adverse health effects. Basically, e-noses are able to discriminate odor (or VOC) patterns from sets of sensors' responses. Although their ultimate goal is not to separate and identify VOCs in the pattern, as gas chromatography/mass spectrometry (GC-MS) does, their characteristics make them promising candidates for discriminating healthy versus sick population samples from the signals patterns from sensors (fingerprints). The literature shows that e-noses have been successfully applied to the discrimination of patients with cancer and other diseases from healthy controls [10]–[17]. As an example, in [18] a low-cost e-nose based on breath analysis with 5 metal oxide semiconductor (MOX) gas sensors was developed for non-invasive diagnosis of chronic obstructive pulmonary disease (COPD) and lung cancer. Classification of patients and controls was produced in a post-processing step by ensemble learning methods. In [19] an e-nose with 6 MOX gas sensors was developed for prostate cancer diagnosis based on urinary VOCs; classification predictions have been obtained by a post-processing learning algorithm based on Boruta algorithm. In [20] an array of 5 MOX sensors was used for the discrimination of lung cancer patients and at-risk healthy subjects based on breath analysis; support vector machine (SVM) and AdaBoost algorithm have been used. Exhaled breath samples have also been analyzed in an e-nose based on 7 MOX gas sensors and various classifiers (linear discriminant analysis - LDA, support vector machine - SVM, and multilayer perceptron - MLP) developed in [21] for lung cancer diagnosis. Breathprints have also been used for lung cancer detection in the e-nose developed by [22], where an array of gas sensors based on different sensing technologies was used.

In this paper, an e-nose devoted to the human volatilome fingerprinting of different matrices (breath or biofluids) is presented. Its codename is SPYROX and it was designed as a portable, standalone, and versatile system for disease detection as well as for human biomonitoring to assess health risk in population [23]–[25].

II. Electronic Nose Implementation

A. System Overview

A block diagram depicting the architecture of the implemented system is shown in Fig. 2. The SPYROX e-nose consists of an automation/control system for air flow and VOC sampling, a power module, a gas-sensor array, and an electronic mainboard, all housed in a transparent plexiglass case. The choice of this material is purely aesthetic and, as detailed in the following sections, it is not exposed in any way to the VOCs of the analyzed sample. The operation of the device, along with the data logging and analysis, can be managed by a Raspberry-PI-based embedded computer through a 7″ touch panel. This embedded computer includes the operating system and the software environment for data analysis. Alternatively, data can be also retrieved by connecting an external personal computer (PC) through the USB/serial link. A specific design choice consisted in separating the gas-sensor array, implemented on the sensor module daughterboard, from the read-out and processing electronics, implemented on the Multisense V2 mainboard. Thanks to this choice, different sensor modules can be used with the same mainboard, making the device flexible for use in different sensing applications.

Fig. 2 and Fig. 3 depict a block diagram and a photo of the Multisense V2 mainboard, respectively. A detailed description of the mainboard can be found in [26]. Briefly, the mainboard provides 10 resistance channels and 10 voltage channels for read-out from chemiresistive gas sensors and voltage read-out from generic sensors. The sensor module hosts 6 commercial micro-electro-mechanical systems (MEMS) MOX-based gas sensors on SMD (surface-mount device) package. Thanks to the MEMS technology, the size and fabrication costs of sensors are significantly reduced and this leads to smaller and cheaper sensing devices [27]. In addition to the 6 SMD sensors, a pair of sockets for sensors in 4 pin through-hole TO-5 packages, was provided, with a final array configuration of 8 sensors. Since the sensor module is removable, the benefit of easy hardware replacement was given, as the sensors degrade their performances due to aging. As shown in Fig. 2, dual-mode sampling is performed, allowing sampling of breath from collection bags (usually made of Tedlar) or headspace from a gas-tight vial containing a liquid or solid biosample. In addition, SPYROX can sample ambient air for application

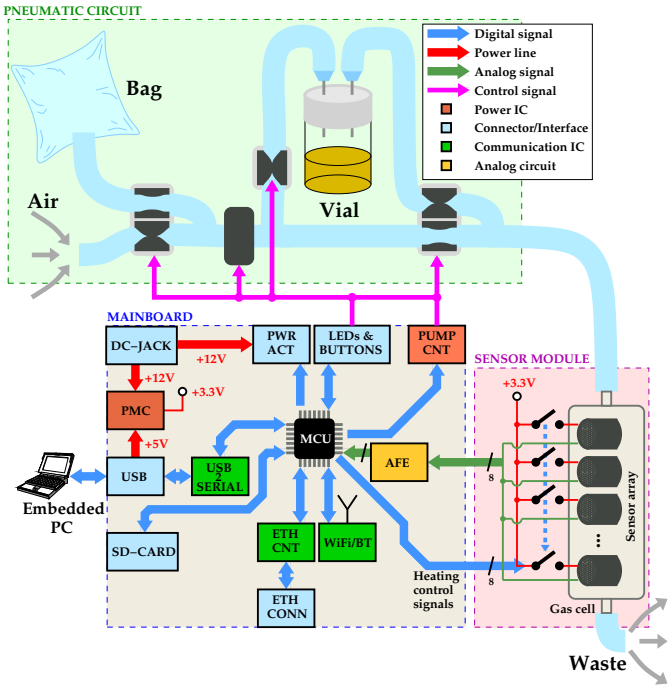

Fig. 2. Architecture of the implemented e-nose.

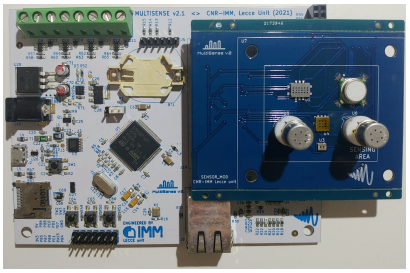

Fig. 3. Photo of the realized Multisense V2 mainboard (white soldermask) with the sensor module inserted (blue soldermask).

in continuous environment air monitoring. Although in the described application the 8-sensor array is operated at constant temperature, the system also supports the temperature modulation operation by driving the sensors' integrated heaters with pulse width modulation (PWM) signals. A piezo-pump controller provides the circuit for interfacing a piezoelectric micropump (mod. mp6-air, Bartels Mikrotechnik GmbH), which offers gas transportation at a controlled flow. A section for serial/USB communication, a slot for the micro-SD card mass memory, a module for WiFi connectivity for sending data remotely, and a module for Ethernet connectivity ensure all useful connectivity solutions. The device is thus ready for data transmission for Internet-of-things (IoT) or cloud frameworks.

B. Proposed Analog-Front End (AFE) Circuit Design

The AFE section represents the interface between the MCU and the sensor module. The latter module mounts the MOX-based chemiresistive gas sensor array, whose working principle is based on electrical resistance changes of sensing layers in response to gases and volatiles [27]. As the sensor's resistance can vary over several decades [28], a circuit based on a multi-

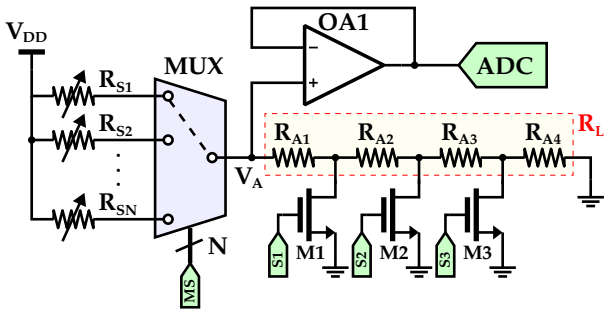

Fig. 4. Circuit schematic of a voltage divider with multi-ranging approach. As an example, the R_{S1} is selected through the multiplexer.

TABLE I
VALUES OF SELECTED RESISTORS.

R_{A1}	1 kΩ
R_{A2}	9 kΩ
R_{A3}	90 kΩ
R_{A4}	900 kΩ

TABLE II
ALLOWED CONFIGURATIONS FOR MOSFETS' GATE SIGNALS AND CORRESPONDING LOAD RESISTOR VALUE. L AND H STAND FOR LOW-LEVEL AND HIGH-LEVEL GATE SIGNALS, RESPECTIVELY.

S1	S2	S3	R_L
L	L	L	1 MΩ
L	L	H	100 kΩ
L	H	L	10 kΩ
H	L	L	1 kΩ

ranging voltage divider, whose basic architecture is shown in Fig. 4, was designed for a proper read-out in the wide resistance range. Multi-ranged voltage divider circuits are widely adopted in MOX sensors applications and they are also suggested by sensors' manufacturers as a way to promptly connect the sensors to the MCU while maintaining a low cost, a low design effort, and low parts count on PCB. Such circuits are appropriate for MOX sensors since these exhibit a large change in the resistance value [29]. Auto ranging is an often overlooked critical aspect of sensor read-out interfaces. However, the datasheets of the sensors do not provide any suggestions on how to correctly perform a scale change without losing accuracy or continuity in the sensor read-out signal, nor has this ever been a topic of discussion in the scientific literature. Thus, the proposed theoretical derivation aims to define a general approach to properly shift the resistance range while optimizing the read-out sensitivity in the whole dynamic range. Fig. 4 includes the sensors, R_{S1}, R_{S2}, …, R_{SN}, that are connected between the circuit's supply voltage V_{DD} and a load resistor, R_L, through an analog multiplexer (MUX). The R_L load resistor is made of 4 selectable values, R_{A1}, R_{A2}, R_{A3} and R_{A4}, whose values are reported in TABLE I.

The circuit's output voltage, V_A, is buffered by means of the OA1 operational amplifier (opamp) in voltage follower configuration and it is converted in the digital domain through the ADC integrated in the MCU. The MCP6021 opamp, manufactured by Microchip Technology Inc., was selected since it has a very good noise performance of $8.7\,\mathrm{nV}/\sqrt{\mathrm{Hz}}$

at 10 kHz (typical), and an high gain-bandwidth product of 10 MHz allowing the adoption of the board for a wide range of sensing applications. The MCU provides a successive-approximation ADC with maximum resolution of 12 bits and maximum sampling rate of 2.4 Msps. Considering R_S as the generic value of a selected sensor, the output voltage, V_A, is obtained through the voltage divider's rule as follows:

$$V_A = V_{DD} \cdot \frac{R_L}{R_S + R_L} \tag{1}$$

where the V_{DD} voltage is equal to 3.3 V. The load resistor's value, R_L, is changed with discrete steps through M1, M2 and, M3 MOSFETs, operated as switches, to match the resistance value of the sensor. The allowed MOSFETs configurations, along with the corresponding values of R_L, are reported in TABLE II. The automated change of R_L aims to maximize the absolute sensitivity of the voltage divider circuit, defined as the amount of change in the output, i.e., the output voltage V_A, in response to a change in the input, i.e., the sensor's resistive value R_S. It is worth pointing out that the hereafter derivation only aims to the maximization of AFE's sensitivity. Indeed, the sensitivity of gas sensor depends on intrinsic properties of the gas-sensing material and on operating modes linked, for example, to the working temperature of the sensor set through its integrated heater. The absolute sensitivity of the voltage divider is obtained as follows:

$$S(V_A, R_S) = \left| \frac{\partial V_A}{\partial R_S} \right| = \frac{V_{DD} \cdot R_L}{(R_S + R_L)^2} \tag{2}$$

The (2) is also called differential sensitivity since it is defined as a derivative and it is measured in $\mathrm{V}\,\Omega^{-1}$. From (2), it can be deduced that the absolute sensitivity is maximized as R_S matches R_L [29]. In the proposed multi-ranging approach, the load resistor value, R_L, is selected to maximize the read-out sensitivity across 4 ranges of different order of magnitude. An optimal multi-ranging approach was developed to programmatically switch between adjacent ranges, as the voltage V_A crosses the high threshold V_{TH} or the low threshold V_{TL} voltages. Thanks to this, the maximum read-out sensitivity is guaranteed over the full read-out range.

For small variations ΔR_S of R_S, the following approximate definition of absolute sensitivity is considered:

$$S(V_A, R_S) \approx \left| \frac{\Delta V_A}{\Delta R_S} \right| \tag{3}$$

Regarding the variation of the voltage divider's output voltage, ΔV_A, its minimum detectable value is limited by the quantization noise of the ADC and, thus, by the selected resolution of the latter. In general, smaller voltage variations can be digitized by using an higher resolution, in terms of bits, of the ADC. By assuming ΔV_A in (3) as the root mean square (RMS) value of the voltage variation, the signal-to-quantization-noise (SQNR) is derived as follows:

$$SQNR = \frac{(\Delta V_A)^2}{\sigma_Q^2} = \left(\frac{\sqrt{12} \cdot (2^N - 1)}{V_{FS}} \cdot S(V_A, R_S) \cdot \Delta R_S \right)^2 \tag{4}$$

where N is the resolution, expressed in bits, of the ADC, V_{FS} is the full-scale voltage, and σ_Q^2 is the power of the quantization noise. A desirable condition, in order to acquire a valid voltage signal, is to impose the signal power, ΔV_A^2, greater or equal than the quantization noise power, σ_Q^2. This translates to the following condition:

$$SQNR \geq 1 \tag{5}$$

From (5), it is possible to derive the minimum detectable variation of resistance by replacing the (2) in (4), and imposing the SQNR equal to its lower bound, i.e., 1. By expressing the resistance variation, ΔR_S, as $R_S \cdot \epsilon$ and, by considering a V_{FS} equal to the V_{DD} supply voltage, the following equality is obtained:

$$\sqrt{12} \cdot (2^N - 1) \cdot \frac{R_L \cdot R_S}{(R_S + R_L)^2} \cdot \epsilon = 1 \tag{6}$$

From (6), the minimum relative variation of the R_S resistance, ϵ, is obtained as follows:

$$\epsilon = \frac{1}{\sqrt{12} \cdot (2^N - 1)} \cdot \frac{R_S + R_L}{R_S \parallel R_L} \tag{7}$$

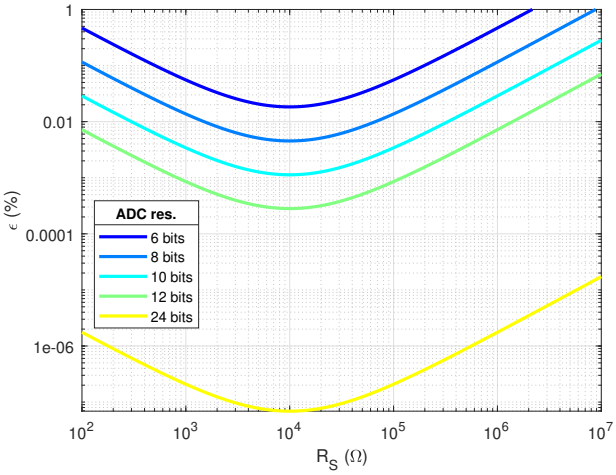

Fig. 5. Smaller detectable variation, ϵ, in percentage for the 10 kΩ range.

Fig. 5 shows the ε function by varying the ADC's resolution with a fixed R_L of 10 kΩ. Here it is compared, in terms of ε, the ADC integrated in the MCU, having selectable resolutions of 6, 8, 10, and 12 bits, with an external 24-bits ADC. As it can be noted, higher resolutions permits to achieve smaller ε. As an example, the external 24-bit ADC would obtain a minimum ε equal to 0.0000069%, i.e., 69 ppb, which results much smaller than 0.028%, i.e., 280 ppm, achieved with the internal 12-bit ADC. However, it is worth pointing out that such high ADC resolution is not necessary in applications where MOX-based gas sensors are involved. The reason can be found by deriving the power of the output noise of the AFE circuit in Fig. 4. By assuming both an ideal MUX and ideal MOSFETs, the small-signal circuit of Fig. 6 can be considered to evaluate the sampled noise power. $\overline{e_m^2}$, $\overline{e_R^2}$, and $\overline{e_O^2}$ are the power spectral densities (PSDs) of the R_S sensor, the R_L load resistor, and the opamp, respectively. The ADC behavior is modeled as a sample-and-hold circuit with sampling frequency equal to f_S,

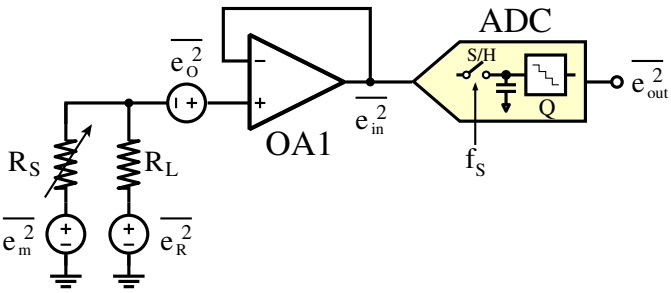

Fig. 6. Small-signal circuit for noise calculation.

followed by a quantizer. The PSD at the input of the ADC can be derived as follows:

$$\overline{e_{in}^2} = \overline{e_m^2} \cdot \left(\frac{R_S}{R_S + R_L}\right)^2 + \overline{e_R^2} \cdot \left(\frac{R_L}{R_S + R_L}\right)^2 + \overline{e_O^2} \quad (8)$$

Regarding $\overline{e_m^2}$ it is known that MOX gas sensors, over controlled conditions in terms of flow and temperature, exhibit noise phenomena. This can be observed in presence of one or more gases and it is caused by adsorption–desorption (AD) noise. This is due to fluctuations in the surface coverage of species adsorbed on the surface of the polycrystalline gas-sensing layer connected to variations in the balance between adsorption and desorption at the sensor working point. This leads to fluctuations in the charge exchange processes between the adsorbate and the sensitive layer, in the heights of the intergrain barriers, and in the final conductivity [30]. An insight on the noise behavior of the AFE circuit comes from a first order approximation of the (8). In particular, only the thermal noise contribution of the MOX gas sensor is considered and, in addition, it is assumed that $R_S = R_L$, i.e., the sensor's value is centered in a specific range. The (8) is simplified as follows:

$$\overline{e_{in}^2} = 2 \cdot k \cdot T \cdot R_S + \overline{e_O^2} \quad (9)$$

An unwanted phenomenon, deriving from the ADC's sampling operation, is the aliasing which causes the folding of noise in the Nyquist bandwidth. The result of the sampling operation is to increases the $\overline{e_{in}^2}$ significantly by a factor equal to $\pi \cdot f_{GBW}/f_S$ [31], where f_{GBW} is the gain-bandwidth product of the opamp. Thus, by multiplying the (9) by the $\pi \cdot f_{GBW}/f_S$ factor and by integrating it from 0 to the Nyquist frequency, i.e., $f_S/2$, the following power of the sampled noise is obtained:

$$v_{out,RMS}^2 = (2 \cdot k \cdot T \cdot R_S + \overline{e_O^2}) \cdot \frac{\pi}{2} \cdot f_{GBW} \quad (10)$$

A constant $\overline{e_O^2}$ of $(8.7\,\mathrm{nV}/\sqrt{\mathrm{Hz}})^2$ and a f_{GBW} equal of $10\,\mathrm{MHz}$ are considered from the MCP6021 datasheet. Assuming a R_S equal to $1\,\mathrm{M\Omega}$, meaning that R_S is centered in the higher maximum range of $1\,\mathrm{M\Omega}$, the worst-case $v_{out,RMS}^2$, equal to $0.13\,\mathrm{mV}^2$, is obtained from (10). By imposing the quantization noise power of the ADC equal to the calculated electronic noise power, $v_{out,RMS}^2$, it can be derived the following ADC's resolution, N, to guarantee a correct conversion

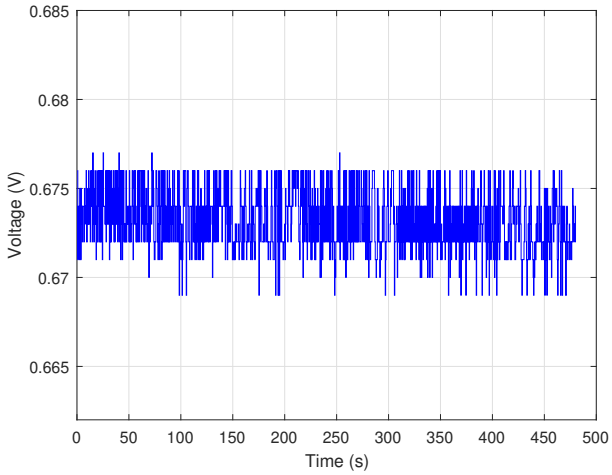

Fig. 7. Voltage measurement from a single gas sensor exposed to 2-butanone.

from the sensor:

$$N = \log_2\left(\frac{V_{FS}}{\sqrt{12} \cdot v_{out,RMS}} + 1\right) \quad (11)$$

By substituting the aforementioned values in (11), it turns out that an ADC with a resolution equal to 11.4 bits is enough for a correct conversion of the signal. As an example, Fig. 7 depicts the voltage measurement from the AFE connected to the TGS2600 sensor during exposure to 2-butanone. The reported measurement was performed with a constant flow of $20\,\mathrm{mL\,min^{-1}}$ at $60\,^\circ\mathrm{C}$. In the real case, a multitude of factors contribute to the sensor's noise power, such as flicker noise, thermal phenomena, flow turbolences, etc. The sum of all the noise contributions result to the measured power equal to $3.3\,\mathrm{mV}^2$ from Fig. 7. This is much higher than the quantization noise power for the 12-bit internal ADC, leading to a required resolution of 9 bits from (11). Although the measured noise power varies with the gas and with the selected range, the noise process is prominent in every measurement.

The (7) is graphically represented in Fig. 8 for the selected values of R_L reported in TABLE II. The overall resistance range from $100\,\Omega$ to $10\,\mathrm{M\Omega}$ was considered with the maximum ADC's resolution for the chosen MCU, which is equal to 12 bits. The red thick curve in Fig. 8 is the resulting ϵ obtained by applying the optimal multi-ranging approach, guaranteeing the minimum relative variation for all resistance ranges. In addition, from Fig. 8, it can be noted that the minimums of ϵ are centered to the R_L values and they have the following expression:

$$\epsilon_{min} = \frac{4}{\sqrt{12} \cdot (2^N - 1)} \quad (12)$$

The concept of resistance and voltage threshold values, between adjacent ranges, is introduced here in order to provide a practical criterion to automatically switch between ranges. This guarantees the minimum detectable variation in every possible resistance range. The hereafter description is referred to Fig. 9, which shows the relationship between read-out resistance range (R_S arrow in the figure) and voltage (V_A line

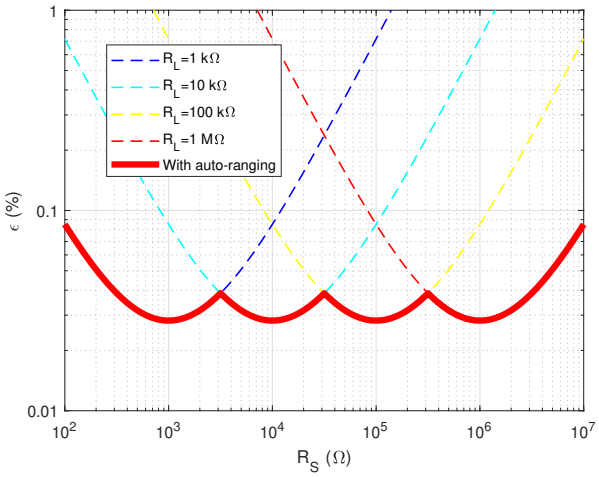

Fig. 8. Smaller detectable variation, ϵ, in percentage from the implemented multi-ranged analog front-end.

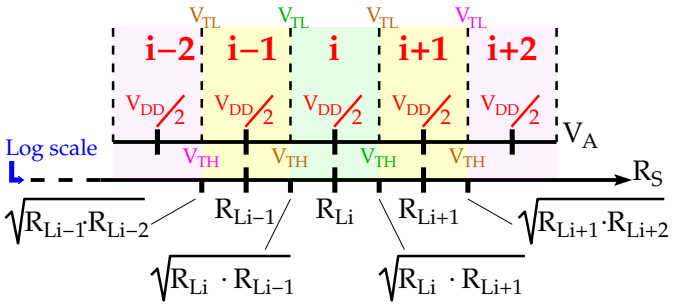

Fig. 9. Voltage and resistance ranges involved in the multi-ranging algorithm.

TABLE III
THRESHOLD RESISTANCE VALUES ($R^{\star}_{i,i\pm1}$)

$R^{\star}_{1,2} = R^{\star}_{2,1}$	3.162 kΩ
$R^{\star}_{2,3} = R^{\star}_{3,2}$	31.62 kΩ
$R^{\star}_{3,4} = R^{\star}_{4,3}$	316.2 kΩ

in the figure) acquired by the ADC. A generic resistance range i, centered at $R_S = R_{Li}$, is considered. Its adjacent ranges are defined as $i \pm 1$ and they are centered at $R_S = R_{L,i\pm1}$. More specifically, $i + 1$ is the higher adjacent range and $i - 1$ is the lower adjacent range. As mentioned earlier, the read-out sensitivity is maximized as the R_S values approach R_{Li}. This condition corresponds to a V_A voltage equal to $V_{FS}/2$ or, in this case, to $V_{DD}/2$. The resistance values, $R^{\star}_{i,i\pm1}$, at which the ϵ curves of the adjacent ranges intersect each other, is obtained by equating the generic ϵ_i curve with its adjacent $\epsilon_{i\pm1}$ curves. These resistance values represent the thresholds, in terms of resistance, between adjacent higher and lower ranges and they can be derived as follows:

$$R^{\star}_{i,i\pm1} = \sqrt{R_{Li} \cdot R_{L,i\pm1}} \tag{13}$$

TABLE III shows the threshold resistance values, obtained by substituting the used load resistor values of TABLE II in (13). At $R^{\star}_{i,i\pm1}$ values, ϵ assumes the following maximum value:

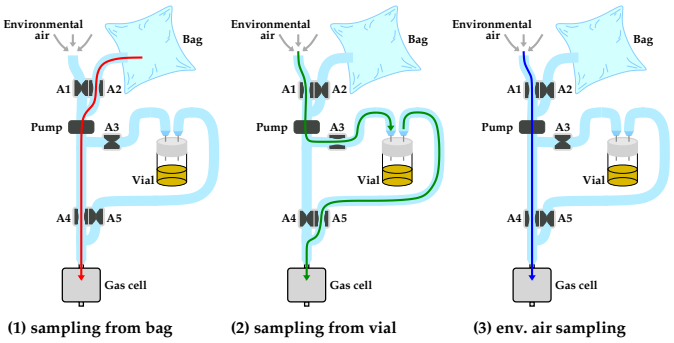

Fig. 10. Operation modes of the implemented pneumatic circuit.

$$\epsilon_{MAX} = \frac{1}{\sqrt{12} \cdot (2^N - 1)} \cdot \frac{(\sqrt{R_{L,i}} + \sqrt{R_{L,i\pm1}})^2}{R^{\star}_{i,i\pm1}} \tag{14}$$

By using the proposed approach, the smaller detectable relative variation, ϵ, is guaranteed to be bounded between ϵ_{min} and ϵ_{MAX} in the input resistance range. They are equal to $0.028\,\%$ and $0.039\,\%$, respectively, for the implemented circuit.

The low and high thresholds voltages for a given i range, $V_{TL,i}$ and $V_{TH,i}$, can be obtained from the voltage divider rule of (1) by considering R_S equal to (13) and R_L equal to R_{Li}. The following expressions can be derived:

$$V_{TL,i} = \frac{V_{DD}}{1 + \sqrt{\dfrac{R_{L,i}}{R_{L,i-1}}}} \tag{15}$$

$$V_{TH,i} = \frac{V_{DD}}{1 + \sqrt{\dfrac{R_{L,i}}{R_{L,i+1}}}} \tag{16}$$

These voltages are used as threshold voltages in the optimal multi-ranging firmware procedure, to switch from a range to the adjacent one and, thus, guaranteeing the smaller detectable relative variation, ϵ, of R_S. Since the adjacent ranges have a constant ratio of the respective $R_{L,i}$ values, the same values of $V_{TL,i} = V_{TL}$ and $V_{TH,i} = V_{TH}$ can be used for switching in all ranges. More specifically, by considering the $R_{L,i}$ values of TABLE II, about $800\,\mathrm{mV}$ and $2.5\,\mathrm{V}$ are obtained for V_{TL} and V_{TH}, respectively.

The read-out of the sensors, along with the multi-ranging algorithm, is performed in circular scanning mode. As the ADC completes a conversion, the next sensor is selected through the analog MUX and the ADC is configured to perform a new signal conversion. An high sampling period of $400\,\mathrm{ms}$, for a complete acquisition cycle, was set. This sampling time has proven to be suitable for the application considering the slow response times of MOX gas sensors [32].

C. Pneumatic Circuit and Modes of Odor Sampling

Fig. 10 depicts the pneumatic circuit of SPYROX, whose programmable configuration implements 3 operating modes: (1) sampling from Tedlar bag, for the analysis of exhaled breath, environmental air, etc; (2) sampling of the headspace odor from a vial, for the analysis of volatile organic compounds (VOCs) gases from biological samples such as blood,

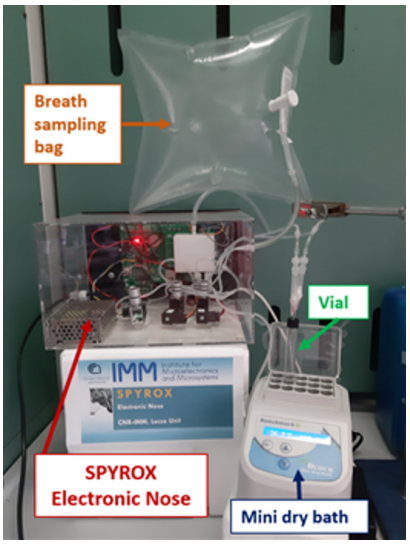

Fig. 11. Photo of SPYROX e-nose.

semen, urine, etc; (3) sampling of air from environment. The sampled odor is transported, through the pipes, in a gas-tight cell on top of the sensor module. The cell was realized in polyoxymethylene (POM), a highly versatile thermoplastic commonly used as engineering material for components machining. The device makes use of 3 pinch solenoid valves (Asco, Emerson Electric Co.). Two of these electrovalves are 3-way (mod. S305 07-ZE30H, one tube normally open, one tube normally closed) and one is 2-way (mod. S104 09-ZE30A, normally closed). The pneumatic circuit is made of flexible (50 shore hardness) pipes (Tygon, Saint Gobain) that are pinched by valves with an external mechanism, so that the fluid only comes in contact with the tubing rather than with the valve. This configuration makes SPYROX e-nose particularly suitable for medical applications, where a very low degree of samples contamination is mandatory. In addition, the circuit comprises the piezoelectric micropump, providing a controlled air flow of $20\,\mathrm{mL/min}$. Depending on the state of these devices, a gas sampling input is selected. With reference to Fig. 10, the following three configurations are allowed:

1) A-2, A-4 opened, all other closed: the gas is sampled from bag;
2) A-1, A-3, A-5 opened, all other closed: the dynamic headspace sampling from a vial is implemented and the environmental air is used as carrier gas;
3) A-1, A-4 opened, all other closed: the environmental air is forced in the gas tight cell. This operation is carried out in order to pre-condition and recover the sensors' resistance to their baseline value.

Fig. 11 shows a photo of the realized SPYROX e-nose with all the components; the designed sensor module, along with the gas tight cell, can be here noticed (see white cube in the plexiglass case). The sensor array is composed by the commercial MOX sensors reported in TABLE IV.

III. Experimental Section

A. Setup Considerations

The suitability of the SPYROX e-nose, for the analysis of human volatilome fingerprints, was tested through a classification test with both single chemical standards and complex mixtures. As for the sampling method, sampling from headspace vial (mode 2 of Fig. 10) was used. In a first instance, chemical aqueous solutions of 12 different analytes were prepared in headspace vials at a concentration of $1\,\mathrm{mg\,mL^{-1}}$. The selected analytes have been proven to be commonly found in human volatilome [23] and are: 1-butanol, heptanal, 2-butanone, 3-pentanone, acetone, ethanol, hexanal, hexane, isoprene, isopropanol, pentanal, pentane. The vial was kept in a mini dry bath (see Fig. 11) and kept at $60\,^{\circ}\mathrm{C}$. Considering the vapor–liquid equilibrium that occur in the headspace vial, the $C^{\star}$ concentration in ppm of the saturated vapours in the vial headspace for each analyte in the prepared solutions at the T temperature, can be calculated as follows:

$$C^{\star} = \frac{P^{\star}}{P^{0}_{atm}} \cdot 10^{6} \cdot \frac{T_0}{T} \tag{17}$$

where P^{0}_{atm} is the atmospheric pressure measured in normal condition, $P^{\star}$ is the saturated vapour pressure of the analyte in solution, and T_0 is the normal temperature. Temperature and pressure in (17) are expressed in K and kPa, respectively. The $P^{\star}$ pressure is obtained from Raoult's law for a single component in an ideal binary solution as follows:

$$P^{\star} = P^{\star}_{pure} \cdot X_{mol} \tag{18}$$

where $P^{\star}_{pure}$ is the vapor pressure of the pure component and X_{mol} its mole fraction in the mixture. The calculated gas concentration of the used analytes varies from a few ppbv to hundreds of ppbv. This range of concentrations is in agreement with that typically found in the breath [33], [34]. As for the classification capabilities of the SPYROX e-nose, more plausible results were obtained by testing some gas mixtures; by considering 3 of the 12 standard chemicals, three binary and one ternary mixtures were realized. Specifically, the following mixtures were prepared in vials by using a concentration of $1\,\mathrm{mg\,mL^{-1}}$ for each substance:

- 1) 2-butanone - hexane;
- 2) acetone - 2-butanone;
- 3) hexane - acetone;
- 4) acetone - 2-butanone - hexane.

Any reactions between the chemical standards in the binary or ternary mixtures considered in the work are unlikely due to the low concentrations involved. They represent a simplified situation of a human biospecimen where hundreds of different VOCs can be present simultaneously.

B. Measurement Procedure

A single sample measurement consists in the following steps:

- A - Pre-conditioning;
- B - Gas exposure and signal acquisition;
- C - Recovery;
- D - Iteration.

TABLE IV
ADOPTED SENSORS.

ID	Sensor	Manufacturer	Declared calibration curves	Heater voltages / power
S1	MiCS-6814 (NH3)	Amphenol SGX Sensortech	Ammonia, ethanol, hydrogen, propane, iso-butane	2.4 V / 76 mW
S2	MiCS-6814 (CO- RED)	Amphenol SGX Sensortech	Carbon monoxide, hydrogen sulfide, ammonia, hydrogen, ethanol, methane, propane, isobutane	1.7 V / 43 mW
S3	MiCS-6814 (NO_2 - OX)	Amphenol SGX Sensortech	Nitrogen dioxide, nitric oxide, hydrogen	2.2 V / 66 mW
S4	AS-MLV-P2	ScioSense	Carbon monoxide, butane, methane, ethanol, hydrogen	3 V / 50 mW
S5	TGS8100	Figaro	Carbon monoxide, ethanol, hydrogen, methane, isobutane	1.8 V / 15 mW
S6	GM-502B	Winsen	Ethanol, formaldehyde, toluene	2.5 V / 50 mW
S7	TGS2600	Figaro	Methane, carbon monoxide, iso-butane, ethanol, hydrogen	5 V / 210 mW
S8	TGS2602	Figaro	Hydrogen, ammonia, ethanol, hydrogen sulfide, toluene	5 V / 280 mW

During step A, environmental air is pumped into the gas cell in order to stabilize the sensors' resistance to their baseline values, R_{air}. This step takes $40\,\mathrm{min}$ and it is carried out by the pneumatic circuit in mode 3 (see Fig. 10). During step B, the pneumatic circuit is set in mode 2 and the odor is pumped, at constant flow, from the vial's headspace into the gas cell. This operation takes $20\,\mathrm{min}$, during which the resistance signals from sensors are acquired by the ADC and are transferred to the embedded computer or to the hard drive of a generic PC through the USB/serial link. The step C is equivalent to step A. Steps B and C are iterated for a total of 5 times.

C. Experimental Results

For all the analytes, an appreciable decrease in the electrical sensor resistance was registered during step B. The sensor array produced response patterns to the different analytes evaluable for the classification. As an example, Fig. 12 shows the sensor's normalized signals versus discrete-time for ethanol. The piezoelectric pump fills, with a low flow of $20\,\mathrm{mL\,min^{-1}}$, the system's dead volume equal to about $35\,\mathrm{cm^3}$. This results in the high response times of Fig. 12. The sensors' ID codes are reported in TABLE IV. The extracted features from curves are the 8-tuples and consist in a complete set of sensors' normalized responses. They are obtained with a sampling rate of $2.5\,\mathrm{Hz}$. The normalization is obtained through dividing the resistance signal, R_S, by the initial baseline resistance during pre-conditioning in air, R_{air}. As extracted features from the normalized responses, the 5 negative peaks of the 8 sensors are taken for the 12 chemical standards. These 8-tuples become the input observations for the training procedure. Fig. 13 summarizes the obtained 60 observations with a radar plot.

To speed up the measurements, the recovery cycles have been stopped before reaching the initial baseline. This premature stop does not represent an issue for the sensing capability

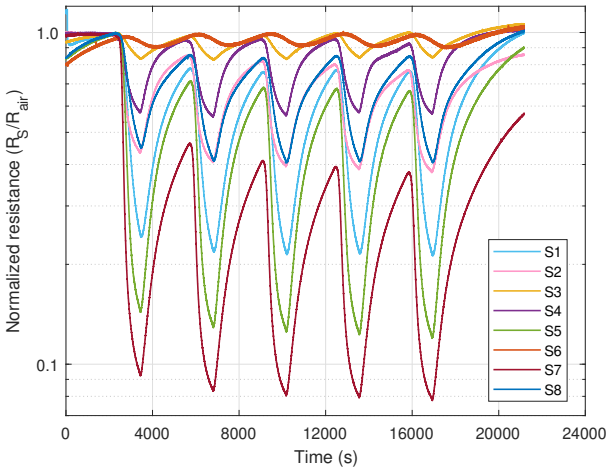

Fig. 12. Sensors' normalized responses versus time under multiple ethanol exposure and recovering in air. The sensors' ID codes are reported in TABLE IV.

of the array since, as it can be noted from Fig. 13, the observations are repeatable over successive exposure cycles. Moreover, as it can be verified from the high classification scores showed below, this measurement approach, that doesn't wait the full recovery of the signal, does not cause any significant information loss in sensors' responses. The extracted observations were used as training dataset of various machine learning (ML) classification models. In this respect, the Classification Leaner app, found in MATLAB, was adopted to explore the performances of classifiers and the results are reported in TABLE V. A 10-fold cross-validation was used to protect the models from overfitting and the following families of classification models were successfully tested: discriminant analysis (linear and quadratic), SVM (linear, quadratic, cubic, fine Gaussian, medium Gaussian, and coarse Gaussian), nearest neighbor classifiers (fine, medium, coarse,

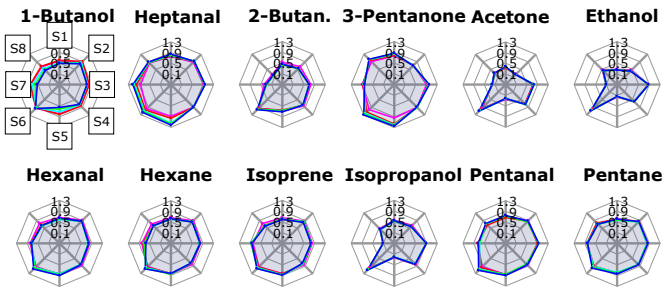

Fig. 13. Radar plot of the normalized responses of sensors for the tested chemical standard. The sensors' ID codes are reported only for 1-Butanol and they are specified in TABLE IV.

TABLE V
ACCURACY REPORTS FROM THE TRAINING OF VARIOUS CLASSIFIERS.

Model	Accuracy
Linear Discriminant	100 %
Subspace Discriminant	93.3 %
Fine KNN	91.7 %
Medium Gaussian SVM	90 %
Linear SVM	86.7 %
Quadratic SVM	85 %
Bagged Trees	85 %
Subspace KNN	85 %
Cubic SVM	83.3 %
Weighted KNN	81.7 %

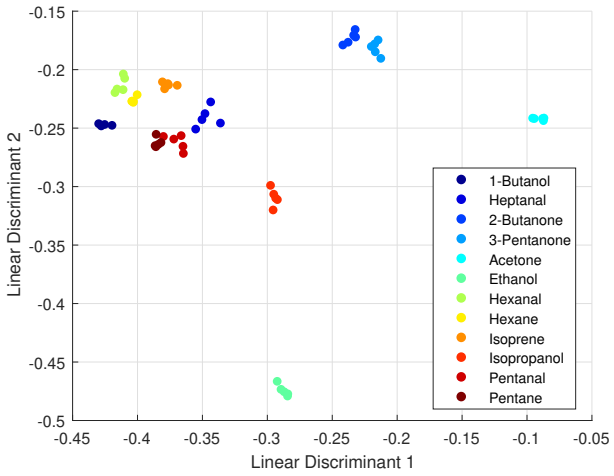

Fig. 14. Plot of the first 2 linear discriminants from single substances.

cosine, cubic, weighted), and ensemble classifiers (boosted trees, bagged trees, subspace discriminant, subspace KNN, and RUSboosted trees). After the training, the accuracy is retrieved for each model. It is calculated on all observations, considering each observation when it was in a held-out fold of the cross-validation procedure. A perfect accuracy of 100% is achieved by the linear discriminant classifier. In this case, all the extracted features from resistance signals are correctly classified into the respective chemical standards. This result is confirmed by the diagram in Fig. 14, showing a good separation of classes while considering the first 2 linear discriminants. The classification capability of the system was further verified by

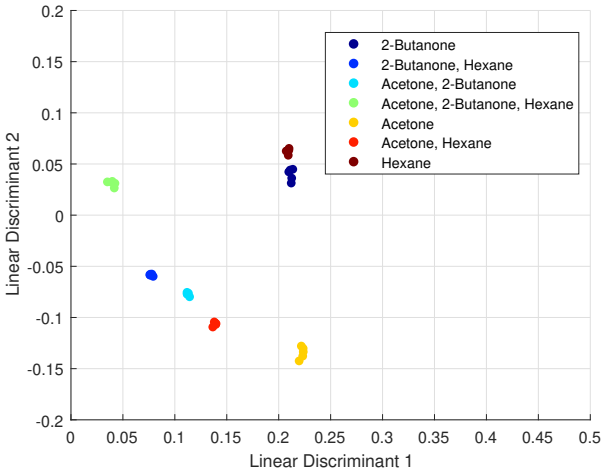

Fig. 15. Plot of the first 2 linear discriminants from mixtures.

testing the binary and ternary gas mixtures already introduced in Sec. III-A. As already done with single chemical standards, 5 measurements (8-tuples) were taken for the 4 mixtures. In addition to these, measurements from single substances (i.e., 2-butanone, acetone, and hexane) in mixtures were added to the dataset. Even in this case, a 100% accuracy was achieved with linear discriminant model. This is confirmed by Fig. 15 which shows the clear separation between classes in the linear discriminants plot.

The main limitation of the study is the lack of a validation step on real human biosamples, that will be a next milestone within pilot studies on sample population approved by Ethical Commitee. In this work the system's design and implementation is emphasized describing the architecture, the hardware, and technological features not usually discussed in the literature or by manufacturers. Therefore, the functionality of the device is tested here with single standards and simple VOC mixtures as it is commonly done in testing procedure as a first step. Indeed, the considered mixtures only are simplified representations of real VOCs from biosamples. As reported in a previous study [23], these are typically complex mixtures with a rich variety of involved VOCs. Longer exposure times may be considered in real applications to avoid any information loss from sensors' resistive responses. However, experimental results obtained by classifying single chemical standards and simple mixtures are promising, especially considering that the analyzed solutions are aqueous. This is close to the real case of exhaled breath that has a high moisture content close to saturation; other more complex human biological liquid matrices (such as blood, urine, saliva, etc.) are also water-based. As shown earlier, classification scores from the developed device are high despite the high presence of water vapour in the headspace of the analysed standard samples. Thus, the presented experimental results give a proof on the system's efficacy to the global fingerprint analysis and classification of some VOCs which are commonly found in human volatilome.

IV. Conclusion

In this paper, an e-nose devoted to the human volatilome fingerprinting of different matrices is presented. The device, code-named SPYROX, adopts an array of 8 commercial MOX gas sensors and it is capable of dealing with breath and headspace analysis of human biosamples. The aim is to implement a low-cost device with accurate data from sensors, eventually leading to high classification scores of single gas species and mixtures in output. The goal is reached by advancing the concept of voltage dividers' range shifting, whose aim is the optimization of the read-out sensitivity over the full dynamic range. Moreover, theoretical derivations proved that a 12-bit integrated ADC is enough for an accurate signal conversion. Other advantages of the proposed electronic nose regard the large variety of connectivity and power options, a compact size for portable and standalone operation, and a modular design for an easy maintenance and flexibility. The functionality of the device was proved by a classification test of chemical standards and VOC mixtures as well. In the first case, 12 chemical standards of real interest in human volatilome analysis were tested. Afterwards, 3 binary mixtures and 1 ternary one were prepared to further test the classification capabilities towards more plausible samples. In both cases, an accuracy of 100% was obtained using a linear discriminant model. This result proves the system's efficacy to the fingerprint analysis of human volatilome.

References

[1] "2022 new cancer cases and cancer deaths on the rise in the EU," ECIS - European Cancer Information System, 2023, accessed [07-11-2023]. [Online]. Available: https://ecis.jrc.ec.europa.eu/pdf/CancerEstimates2022_factsheet.pdf

[2] Y. Y. Broza, R. Vishinkin, O. Barash, M. K. Nakhleh, and H. Haick, "Synergy between nanomaterials and volatile organic compounds for non-invasive medical evaluation," *Chemical Society Reviews*, vol. 47, no. 13, pp. 4781–4859, Jul. 2018.

[3] A. V. Radogna, N. Fiore, M. R. Tumolo, V. D. Luca, L. T. D. Paolis, R. Guarino, C. G. Leo, P. Mincarone, E. Sabato, F. Satriano, S. Capone, and S. Sabina, "Exhaled breath monitoring during home ventilo-therapy in COPD patients by a new distributed tele-medicine system," *Journal of Ambient Intelligence and Humanized Computing*, vol. 12, no. 4, pp. 4419–4427, dec 2019.

[4] L. Cheng, Q.-H. Meng, A. J. Lilienthal, and P.-F. Qi, "Development of compact electronic noses: a review," *Measurement Science and Technology*, vol. 32, no. 6, p. 062002, Apr. 2021.

[5] D. Karakaya, O. Ulucan, and M. Turkan, "Electronic Nose and Its Applications: A Survey," *International Journal of Automation and Computing*, vol. 17, no. 2, pp. 179–209, Apr. 2020.

[6] W. Wojnowski, T. Dymerski, J. Gębicki, and J. Namieśnik, "Electronic Noses in Medical Diagnostics," *Current Medicinal Chemistry*, vol. 26, no. 1, pp. 197–215, 2019.

[7] A. D. Wilson, "Recent progress in the design and clinical development of electronic-nose technologies," *Nanobiosensors in Disease Diagnosis*, vol. 5, pp. 15–27, Jan. 2016.

[8] B. Buszewski, M. Kęsy, T. Ligor, and A. Amann, "Human exhaled air analytics: biomarkers of diseases," *Biomedical Chromatography*, vol. 21, no. 6, pp. 553–566, 2007.

[9] A. H. Jalal, F. Alam, S. Roychoudhury, Y. Umasankar, N. Pala, and S. Bhansali, "Prospects and Challenges of Volatile Organic Compound Sensors in Human Healthcare," *ACS Sensors*, vol. 3, no. 7, pp. 1246–1263, Jul. 2018.

[10] C. Baldini, L. Billeci, F. Sansone, R. Conte, C. Domenici, and A. Tonacci, "Electronic Nose as a Novel Method for Diagnosing Cancer: A Systematic Review," *Biosensors*, vol. 10, no. 8, p. 84, Jul. 2020.

[11] M. V. Farraia, J. Cavaleiro Rufo, I. Paciência, F. Mendes, L. Delgado, and A. Moreira, "The electronic nose technology in clinical diagnosis: A systematic review," *Porto Biomedical Journal*, vol. 4, no. 4, p. e42, Jul. 2019.

[12] A. D. Wilson, "Biomarker metabolite signatures pave the way for electronic-nose applications in early clinical disease diagnoses," *Current Metabolomics*, vol. 5, pp. 90–101, 2017.

[13] E. Westenbrink, R. P. Arasaradnam, N. O'Connell, C. Bailey, C. Nwokolo, K. D. Bardhan, and J. A. Covington, "Development and application of a new electronic nose instrument for the detection of colorectal cancer," *Biosensors & Bioelectronics*, vol. 67, pp. 733–738, May 2015.

[14] P. Bassi, L. D. Gianfrancesco, L. Salmaso, M. Ragonese, G. Palermo, E. Sacco, R. A. Giancristofaro, R. Ceccato, and M. Racioppi, "Improved non-invasive diagnosis of bladder cancer with an electronic nose: A large pilot study," *Journal of Clinical Medicine*, vol. 10, no. 21, p. 4984, Oct. 2021.

[15] A. I. Buma, M. Muller, R. de Vries, P. J. Sterk, V. van der Noort, M. Wolf-Lansdorf, N. Farzan, P. Baas, and M. M. van den Heuvel, "eNose analysis for early immunotherapy response monitoring in non-small cell lung cancer," *Lung Cancer*, vol. 160, pp. 36–43, Oct. 2021.

[16] S. A. Wulandari, R. Pramitasari, S. Madnasri, and Susilo, "Electronic Noses for Diabetes Mellitus Detection: A Review," in *2020 International Seminar on Application for Technology of Information and Communication (iSemantic)*, Sep. 2020, pp. 364–369.

[17] H.-Y. Yang, Y.-C. Wang, H.-Y. Peng, and C.-H. Huang, "Breath biopsy of breast cancer using sensor array signals and machine learning analysis," *Scientific Reports*, vol. 11, no. 1, Jan. 2021.

[18] B. V.A., M. Subramoniam, and L. Mathew, "Detection of COPD and lung cancer with electronic nose using ensemble learning methods," *Clinica Chimica Acta*, vol. 523, pp. 231–238, Dec. 2021.

[19] L. Capelli, C. Bax, F. Grizzi, and G. Taverna, "Optimization of training and measurement protocol for eNose analysis of urine headspace aimed at prostate cancer diagnosis," *Scientific Reports*, vol. 11, no. 1, Oct. 2021.

[20] D. Marzorati, L. Mainardi, G. Sedda, R. Gasparri, L. Spaggiari, and P. Cerveri, "MOS sensors array for the discrimination of lung cancer and at-risk subjects with exhaled breath analysis," *Chemosensors*, vol. 9, no. 8, p. 209, Aug. 2021.

[21] J.-E. Chang, D.-S. Lee, S.-W. Ban, J. Oh, M. Y. Jung, S.-H. Kim, S. Park, K. Persaud, and S. Jheon, "Analysis of volatile organic compounds in exhaled breath for lung cancer diagnosis using a sensor system," *Sensors and Actuators B: Chemical*, vol. 255, pp. 800–807, Feb. 2018.

[22] W. Li, Z. Jia, D. Xie, K. Chen, J. Cui, and H. Liu, "Recognizing lung cancer using a homemade e-nose: A comprehensive study," *Computers in Biology and Medicine*, vol. 120, p. 103706, May 2020.

[23] V. Longo, A. Forleo, A. Ferramosca, T. Notari, S. Pappalardo, P. Siciliano, S. Capone, and L. Montano, "Blood, urine and semen Volatile Organic Compound (VOC) pattern analysis for assessing health environmental impact in highly polluted areas in Italy," *Environmental Pollution*, vol. 286, p. 117410, Oct. 2021.

[24] V. Longo, A. Forleo, L. Giampetruzzi, P. Siciliano, and S. Capone, "Human Biomonitoring of Environmental and Occupational Exposures by GC-MS and Gas Sensor Systems: A Systematic Review," *International Journal of Environmental Research and Public Health*, vol. 18, no. 19, p. 10236, Sep. 2021.

[25] V. Longo, A. Forleo, A. V. Radogna, P. Siciliano, T. Notari, S. Pappalardo, M. Piscopo, L. Montano, and S. Capone, "A novel human biomonitoring study by semiconductor gas sensors in Exposomics: investigation of health risk in contaminated sites," *Environmental Pollution*, vol. 304, p. 119119, Jul. 2022.

[26] A. V. Radogna, S. Capone, L. Francioso, P. A. Siciliano, and S. D'Amico, "Performance analysis of an mls-based interface for impulse response estimation of resistive and capacitive sensors," *IEEE Transactions on Circuits and Systems I: Regular Papers*, vol. 69, no. 9, pp. 3666–3678, 2022.

[27] A. V. Radogna, S. Capone, L. Francioso, P. A. Siciliano, and S. D'Amico, "A 296 nJ Energy-per-Measurement Relaxation Oscillator-Based Analog Front-End for Chemiresistive Sensors," *IEEE Transactions on Circuits and Systems I: Regular Papers*, vol. 68, no. 3, pp. 1123–1133, 2021.

[28] F. Ciciotti, C. Buffa, A. V. Radogna, L. Francioso, S. Capone, R. Gaggl, and A. Baschirotto, "A 450 μA 128-dB Dynamic Range A/D CMOS Interface for MOX Gas Sensors," *IEEE Sensors Journal*, vol. 19, no. 24, pp. 12 069–12 078, 2019.

[29] K. Arshak, G. Lyons, L. Cavanagh, and S. Clifford, "Front-end signal

conditioning used for resistance-based sensors in electronic nose systems: a review," *Sensor Review*, vol. 23, no. 3, pp. 230–241, Sep. 2003.
[30] S. Gomri, T. Contaret, J. Seguin, K. Aguir, and M. Masmoudi, "Noise modeling in MOX gas sensors," *Fluctuation and Noise Letters*, vol. 16, no. 02, p. 1750013, Mar. 2017.
[31] R. Schreier, J. Silva, J. Steensgaard, and G. Temes, "Design-oriented estimation of thermal noise in switched-capacitor circuits," *IEEE Transactions on Circuits and Systems I: Regular Papers*, vol. 52, no. 11, pp. 2358–2368, 2005.
[32] J. Burgués and S. Marco, "Wind-independent estimation of gas source distance from transient features of metal oxide sensor signals," *IEEE Access*, vol. 7, pp. 140 460–140 469, 2019.
[33] W. Hu, W. Wu, Y. Jian, H. Haick, G. Zhang, Y. Qian, M. Yuan, and M. Yao, "Volatolomics in healthcare and its advanced detection technology," *Nano Research*, vol. 15, no. 9, pp. 8185–8213, jun 2022.
[34] N. Drabińska, C. Flynn, N. Ratcliffe, I. Belluomo, A. Myridakis, O. Gould, M. Fois, A. Smart, T. Devine, and B. D. L. Costello, "A literature survey of all volatiles from healthy human breath and bodily fluids: the human volatilome," *Journal of Breath Research*, vol. 15, no. 3, p. 034001, apr 2021.

Antonio Vincenzo Radogna (Member, IEEE) received the M.Eng. degree in electronic engineering from the University of Parma, Parma, Italy, in 2012, and the Ph.D. degree in complex systems engineering from the University of Salento, Lecce, Italy, in 2021. From 2012 to 2017, he was an Electronic Engineer mainly in the Ambient Assisted Living (AAL) and renewable energies industries. From 2017 to 2023, he was a Research Fellow with the Institute for Microelectronics and Microsystems (IMM), National Research Council (CNR), Lecce. Since 2023, he has been with the Department of Experimental Medicine, University of Salento, where he is serving as an Assistant Professor. His current research interests include the design of CMOS integrated read-out interfaces for sensors, biomedical electronic circuits for healthcare, e-noses development, and industrial sensing technologies. Dr. Radogna joined the committee of the 2023 International Conference on IC Design and Technology (ICICDT) as publication chair.

Giuseppe Grassi received the laurea degree in Electronic Engineering (with honors) from the Università di Bari, Bari, Italy, and the Ph.D. degree in Electrical Engineering from the Politecnico di Bari, Bari, Italy, in 1994. In 1994 he joined the Dipartimento di Ingegneria dell'Innovazione, Università del Salento, Lecce, Italy, where he is currently a Professor of Electrical Engineering. His research interests include complex systems,synchronization properties and chaos-based cryptography, dynamics of nonlinear systems, artificial intelligence, neural networks applied to wind and photovoltaic systems. He has published 148 papers in international journals (source: Web of Science) and about 100 papers in proceedings of international/national conferences. From 2008 to 2011 he served as an Associate Editor for the IEEE Transaction on CAS-II. From 2010 to 2013 he served as an Associate Editor of the IEEE CAS Magazine. He is a Senior Member of IEEE and a member of the IEEE Technical Committee on Nonlinear Circuits and Systems. From January 2012 to Juanuary 2016 he served as the Director of the Centro Cultura Innovativa d'Impresa, a interdepartmental center of the Università del Salento with an annual budged of over 10 millions euros in researches on emerging technologies. From Juanuary 2016 to Juanuary 2019 he served as the Head of the Department of Engineering for Innovation at the Università del Salento. Since November 2019 he serves as a Pro-Vice Chancellor for Administration and Finance.

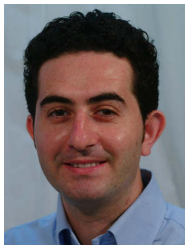

Stefano D'Amico (Senior Member, IEEE) was born in Lecce, Italy, in 1976. He received the Laurea degree in Electronic Engineering from the Politecnico di Bari, Bari, Italy, in 2001. He received the Ph.D. degree in Microelectronics from Istituto Superiore Universitario per la Formazione Interdisciplinare, (ISUFI), Lecce, Italy. From 2007 he served the Università del Salento (Lecce, Italy), Dipartimento di Ingegneria dell'Innovazione as Assistant Professor in Electronics. Since 2015 he serves the same University as Associate Professor. His research interests focus on the design and testing of analog filters, data converters, sensor interfaces, and circuits for power management. Since 2002 he has authored or co-authored more than 160 papers in international journals or conferences proceedings, 7 book chapters and 4 international patents. He joined the Technical Program Committee of different international conferences: ESSCIRC (since 2016), IEEE ICICDT (since 2012) and IEEE PRIME (since 2012). He was General Chair of the ICICDT 2019. In 2015 he co-founded Thetis Microelectronics srls, a start-up company operating in the semiconductors field.

Pietro Aleardo Siciliano received the degree in Physics from the University of Lecce in 1985 and the Ph.D. degree in Physics from the University of Bari in 1989. For 20 years he was the Director of research with the Institute for Microelectronics and Microsystems (IMM), National Research Council (CNR), Lecce, where he has been working in the field of sensors, MEMS, and microsystems for many years. He has authored about 350 scientific articles. He is a referee and a member of the advisory board of international journals. He is a member of the Steering Committee of AISEM, the Italian Association on Sensors and Microsystems. He has been the chairman and a member of the organizing committee of international conferences and schools in sensors and microsystems area. He is the President of the Italian Association on Ambient Assisted Living, responsible for INNOVAAL, the Public–Private Partnership on Active and Assisted Living, and the President of the National Technological Cluster for Smart Living Technologies. He has been responsible for several national and international projects at IMM-CNR.

Angiola Forleo graduated in Physics in 2000 at the University of Lecce. Since 2000 she joined the Institute for the Microelectronic and Microsystems (CNR-IMM) in Lecce, being involved on the electrical/functional characterization of novel nanostructured materials and hybrid organic/inorganic materials for gas sensors application. From 2010 she gained a researcher permanent position in the same institute. Her research activities concern gas sensor systems for applications in biomedical, environmental, industrial, agrifood and life sciences sectors, and the development of analytical chemical methods based on SPME/GC-MS for the analysis of complex gaseous and volatile mixtures in different biological, food and environmental matrices to support gas sensors. Recent interests regard disease screening and human biomonitoring based on combined use of SPME/GC-MS and electronic noses, VOC analysis in human biospecimen (breath, blood, urine, semen, saliva), as well as the investigation of cell culture Volatilomes. She is coauthor of several peer reviewed papers and many conference proceedings. She is actively involved in several projects and collaborations.

Simonetta Capone graduated in Physics (summa cum laude) in 1996 and in 2000 she received her Ph.D. in Physics at the University of Lecce. Since 2002 she is a researcher at the National Research Council - Institute for the Microelectronic and Microsystems (CNR-IMM) in Lecce, Italy, leading the Sensor Characterization Lab. She contributes to the development and electrical/functional characterization of chemical sensors and new technological solutions for chemical sensing. Her research activities are also devoted to the Integration of singles sensors in Devices and sensor arrays in Electronic Noses. Her current research interests are: a) development of multifunctional sensor systems for the analysis of exhaled breath as well as biological samples (urine, blood, human semen, saliva, etc.) of patients with diseases (chronic respiratory problems, cancers and neurodegenerative diseases, metabolic alterations) for medical diagnostics, screening, as well as patient monitoring and stratification; b) development of devices based on chemical sensors equipped with low power sensor interface; c) development of advanced chemical analytical methods by SPME/GC-MS coupled to a gas sensor detector; d) investigation of cell culture Volatilomes as bottom-up approach to identify biomarkers of pathologic conditions and to study the metabolic pathways that produce such compounds; e) human biomonitoring based on combined use of SPME/GC-MS and electronic noses. She is co-author of more than 100 peer reviewed publications and numerous proceedings. She is a research unit coordinator for CNR-IMM in several projects.